0.1 Untersuchungen von Hadronstruktur und Hadronspektroskopie

COMPASS-Kollaboration , davon Mitarbeiter des Inst. f. Kernphysik, Mainz:
K. Dehmelt , J. Ehlers , D. von Harrach , R. Hermann , A. Huf , E.M. Kabuß , A. Korzenev , M. Leberig , G.K. Mallot , J. Pochodzalla , Y. Puhach , Th. Walcher , J. Zhao ,

Abstract. The NA58 experiment has been set up by the COMPASS collaboration at the CERN SPS M2 beam line to study hadron structure and hadron spectroscopy using high energy muon and hadron beams. The main goal of the muon programme is the measurement of the gluon polarisation in the nucleon via photon gluon fusion in polarised quasi-real photo absorption.

Data taking started in 2002. First results are obtained on inclusive asymmetries, transverse Collins asymmetries, vector meson production, Λ polarisation, high p_{T} hadron pairs and open charm production.

0.1.1 The COMPASS experiment

The COMPASS experiment [1] is a fixed target experiment (NA58) for the investigation of hadron structure and spectroscopy at the M2 beamline of the CERN SPS. Measurements with hadron and muon beam with energies between 100 and 200 GeV are being performed. The main goal of the experiments with the muon beam is the investigation of the spin structure of the nucleon to determine the contribution of gluons to the spin of the nucleon and to perform a first measurement of the transversity structure function in the COMPASS kinematic range. With hadron beams, measurements will focus on the polarisability of pions and kaons, glue ball searches, semileptonic decays of charmed hadrons and on double-charmed baryons.

Currently the experimental setup is optimised for the measurement of the gluon polarisation with the help of photon-gluon fusion in the quasi-real photon regime and the deep inelastic scattering regime.

The COMPASS collaboration joins about 220 physicists from 27 institutes from Europe, Russia, Japan and India. The experiment was constructed in 1998 – 2000 and commissioned in 2001. The years 2002 and 2003 were the first physics runs. Data were taken with 160 GeV/c muons at an intensity of $2 \cdot 10^8$ muons per spill of 4.8 s. The 80% polarised muons scattered of a polarised LiD target made out of two cells of 60 cm length polarised in opposite directions.

The detector (see fig. 1) is conceived as a two-stage spectrometer. The large angle spectrometer just downstream of the target covers an aperture of ± 180 mrad while the small angle spectrometer detects particles within the inner ± 30 mrad. Both sections comprise tracking and particle identification detectors grouped around conventional dipole magnets providing field integrals of 1 and 4.4 Tm, respectively.

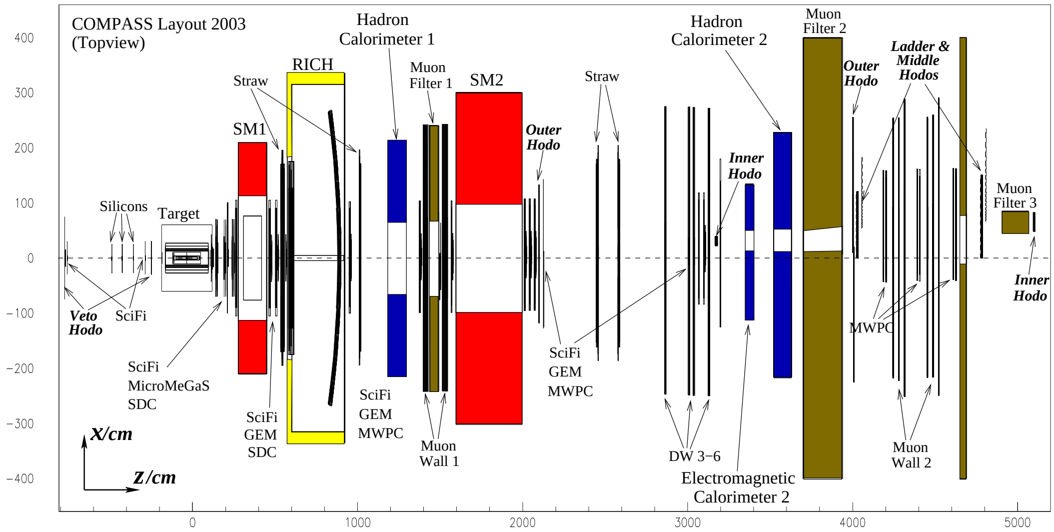

Abb. 1: Schematic drawing of the COMPASS experiment. Shown is the 2003 setup.

0.1.2 The trigger system

The hodoscope system

The trigger system [2, 5] for the muon programme was developed by the groups from Mainz and Bonn. It bases on the detection of the scattered muons in coincidence with the produced hadrons. Information from up to 10 trigger scintillation hodoscopes located in the small angle spectrometer and from two hadron calorimeters form a trigger signal on the basis of target pointing and energy loss within 500 ns [3].

For the 2002 run the two outer hodoscopes (H3O and H4O) were added to the trigger system to cover the large Q^2 region up to 20 GeV^2. The upper Q^2 limit is fixed by the size of the gap of the second spectrometer magnet. The hodoscopes use horizontal strips for vertical target pointing. To gain the neccassary precision for the outer system a large lever arm is needed. Thus, H3O is mounted directly behind the second spectrometer magnet. It has a large central hole to avoid too high rates in the 7 cm wide strips as this region is anyway covered by the other hodoscope systems. H4O is mounted behind the muon filter to facilitate muon identification.

All hodoscope elements have a similar layout of their electronics. They are read out by photomultipliers and the signals are discriminated in constant fraction discriminators. For elements with PMs at both sides the signals are fed into meantimers. Afterwards the signals enter a coincidence matrix to select hit combinations belonging to tracks originating in the target or to tracks with an energy loss larger than a minimal energy loss.

The locations of the trigger components are shown in fig. 2. Fig. 3 illustrates the hodoscope pairs and the corresponding trigger matrix pattern used for triggering in standard data taking in 2003.

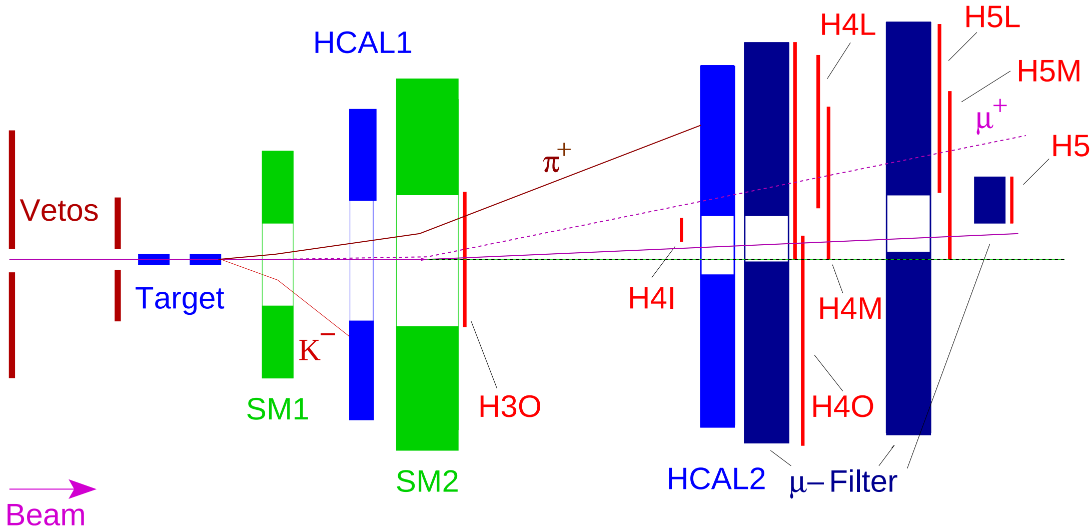

Abb. 2: Location of the components relevant for the trigger.

To facilitate measurements with such an inclusive trigger a veto system is needed due to the high rate of halo muons in the trigger hodoscopes. For the 2003/03 data taking the existing veto system was enlarged with large area scintillation counters to veto halo muons passing through the large area trigger hodoscopes.

LED pulser system

The time calibration of the trigger hodoscope system is usually done using the muon beam. A pulser system would offer a faster and more simple way to perform the calibration, even without the muon beam. In addition it could be used to monitor the performance of the hodoscope system during data taking.

This requires light pulses simulating the shape and the spectrum of those of scattered muons. For the 2003 data taking a prototype LED pulser system was developed [4]. It makes use of ultra bright blue NSPB500 LEDs from Nichia. The GaN semiconductor provides a high efficiency about 10 % in the current to light conversion. The intensity of such LED is about 3400 mcd for 20 mA. The spectrum is centered around 470 nm.

To drive the LED a Mindspeed MC2042-4 LED Laser driver chip was selected normally used for optical network applications. It has special features like a peaking circuit and a clamping function. Using these properties a good approximation of the muon signals in the scintillator was obtained. Figure 4 a) shows the typical photomultiplier signal produced by the LED pulser. The light is transferred to the scintillator by a 1 mm optical plastic fibre. The input of the LED driver accepts the PECL signals with pulse widths $\geq$ 1ns. Using the clamping function a fall time of the PM signal of 26 ns was obtained. The amplitude of the PM signal can be set by changing the pulse width on the Mindspeed driver input. In fig. 4 b) the achieved time jitter of 100 ps for test measurements is illustrated while about 150 ps is acceptable for trigger monitoring and calibration purposes.

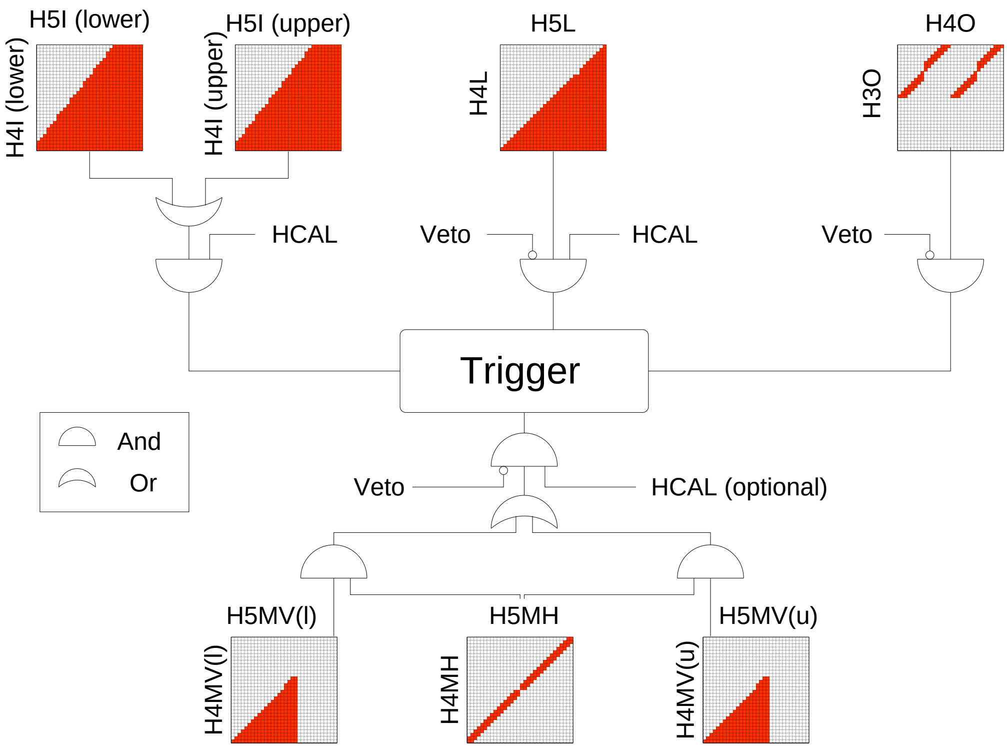

Abb. 3: Hodoscope combinations amd matrix pattern used for data taking.

A system of 32 LED pulser prototypes was produced and installed at middle hodoscope system. Signals were transmitted using twisted pair network cables. Correlated electrical pulses were generated by 2 standard matrix boards. The time difference between the correlated signals can be varied from 0 to 44 ns. In fig. 5 a typical trigger matrix response is shown. With this system the calibration for 58 pixels of middle inclusive trigger obtained with the muon beam was cross checked and the stability of the matrix system monitored. The drifts of delays of the trigger matrix were found to be mainly correlated with the temperature and they are below 200 ps.

The calorimeter trigger

In addition to the selection of scattered muons the trigger system makes use of the hadron calorimeters (HCAL1 and HCAL2) to select events where hadrons were produced in the interaction. The two calorimeters are sandwiched iron-scintillator modules with wavelength shifter and photomultiplier readout. The energy deposited in a 60×60 cm^2 area for HCAL1 or 80×80 cm^2 area for HCAL2 are summed together. If the energy is above a certain threshold in either HCAL, a signal is produced and combined together with the hodoscope part of the trigger system to give a trigger signal for the COMPASS experiment.

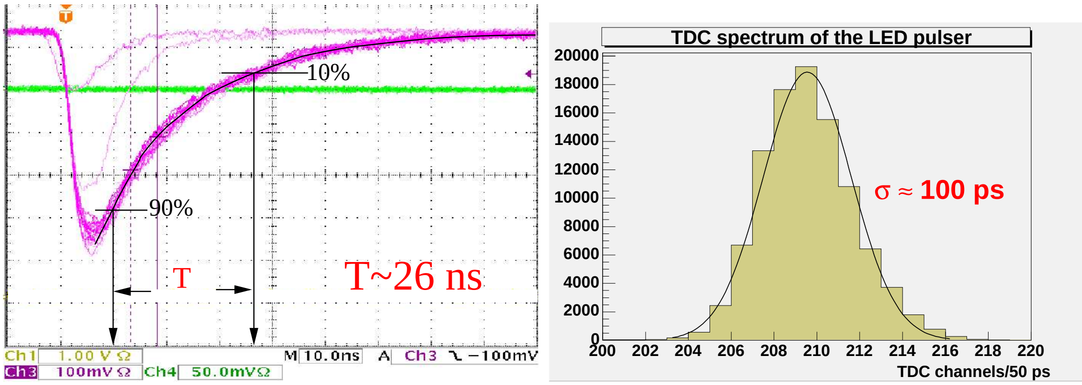

Abb. 4: a) PM response of the Nichia LED driven by the Mindspeed chip. b) TDC spectrum of LED pulser for a 600 mV signal amplitude. The sigma of 100 ps is the best value measured in laboratory. The typical sigma using trigger hodoscopes lies between 250 and 350 ps.

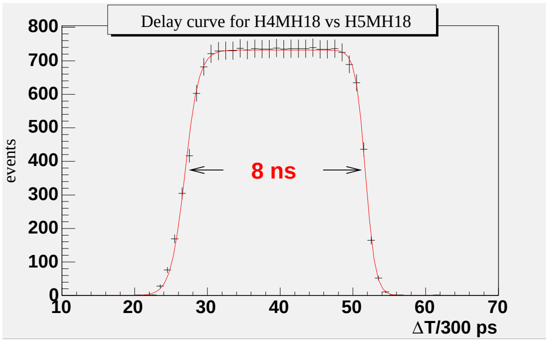

Abb. 5: Response of the middle horizontal matrix versus the time difference between two signals.

The electronics were developed in Mainz and comprise a system of fast analog summation and discriminator modules with good time and energy resolution. For this purpose 5% of the PM signals are split off passively and fed into a first summation stage for summing the signals of a predefind block of 4 calorimeter cells. These signals are transmitted to the trigger barack where the further summation of 4 signals and discrimination takes place. The energy threshold is chosen to be 3 times that of the minimum ionization energy of 160 GeV muon to reject signals produced by scattered muons or the beam halo while keeping most of the hadronic signals. A standalone calorimeter trigger is also used with a higher 9 Mips threshold.

It is obvious that hadrons hitting the border of such predefined blocks would spread their energy over up to four of such blocks with a corresponding loss of the signal to noise ratio. Therefore four layers of predefined blocks are provided which guarantee that each hadron finds one block in which it corresponds to a central event with the full energy deposited in that block. In the beginning of 2002 data taking, the installation of HCAL trigger electronics was complete.

In order to detect and correct problems in the calorimeter trigger a software tool was developed which uses a data stream from the COMPASS DAQ. After processing a certain amount of data, information is extracted for each element of the calorimeter trigger system and a detailed analysis of the quality is done in order to identify possible problems. In 2003 the calorimeter trigger was working very reliable. In addition, a general monitoring software was developed in 2003 to check trigger rates continously and detect deviations e.g. due to temperature effects in real time.

The thresholds in the calorimeter trigger system were monitored continously. The setup of the threshold values is done in the beginning of each year's data taking using alignment data. Here mainly muons are detected. Their energy loss can be used to calibrate the energy scale. Using reconstructed data the preformance of the system was checked. Fig. 6 a) shows the probality that the threshold unit fired versus the track momentum for hadron tracks. The shape of the curve agrees with the expectation based on the knowledge of the fluctuations of the hadronic cluster energies.

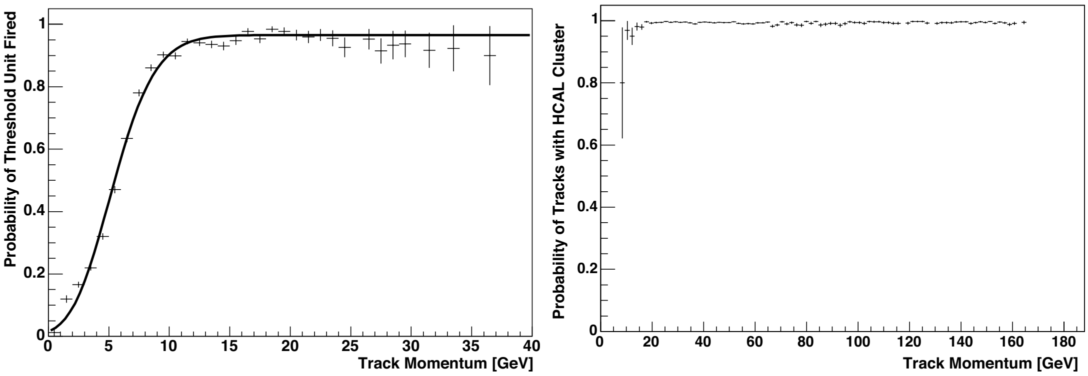

Abb. 6: a) Probability that the threshold units fired versus track momentum, b) probability for muon tracks to produce a cluster in HCAL2 versus momentum.

For an efficient calorimeter trigger, it is important that the HCAL hardware itself is working properly. Analysing 2003 data is is found that the probability for a track entering HCAL to produce an observable cluster is greater than 95% as shown in the fig. 6 b). It is obtained using muons and searching for a cluster close to the tracks projected positon in HCAL2.

Performance

The performance of the trigger system has been studied in detail on the 2002 and 2003 data. The efficiency of the matrix triggers has been determined with help of the standalone calorimetric trigger. Using events with an incoming and a scattered muon one can predict whether the scattered muon fulfills a certain matrix pattern. The ratio of the numbers of events which caused a specific trigger to the predicted ones yields the efficiency of the whole subsystem including scintillator material, light coupling, PM, readout electronics and matrix. Fig. 7 shows as an example the y dependence of the efficiency of the lower part of the inner trigger system. During data taking the matrix was loaded with a pattern for a $y > 0.2$ cut. As can be seen an efficiency of almost 100% is reached for $y > 0.25$ while events with low y are suppressed intentionally.

The global efficiencies for all 4 subsystems were determined with the same method and yield values of above 99 % for the inner and the ladder system, > 97 % for the middle

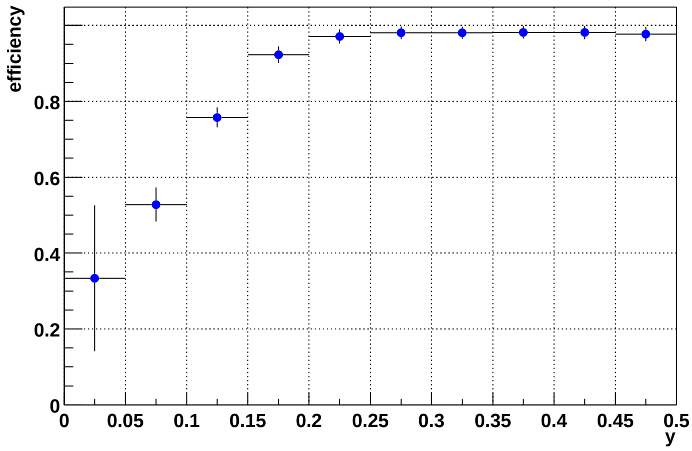

Abb. 7: The efficiency of the lower part of the inner trigger system as a function of the relative energy loss y.

and > 96 % for the outer system. These lower numbers are due to the suppression of the some matrix pixels which are affected by large background contributions.

The kinematic range covered by the trigger system is illustrated in fig. 8. It shows the measured event distribution in y and Q^2 for the 4 hodoscope trigger subsystems. It can be seen that events with small Q^2 (quasi-real photon events) are selected by the inner and ladder system. The cut a low y of between 0.1 and 0.15 is clearly visible for the inner trigger. Together with the ladder trigger the whole y range from 0.2 to 0.9 is covered for small Q^2. The middle and outer trigger mainly select deep inelastic events up to $Q^2 \approx 20$ GeV^2. The range can be further extended towards high Q^2 with the help of the pure calorimetric trigger (see fig. 9).

0.1.3 Data analysis

Analysis of the 2002 data is quite advanced while the reconstruction of the 2003 data is still ongoing. In 2002 57/19 days with longitudinally/transversely polarised target resulted in $3.8 \cdot 10^9$ events and $1.2 \cdot 10^9$ events, respectively.

During the alignment and calibration it turned out that very detailed alignment procedures are needed due to the temperature variations in the experimental area. Therefore work is still in progress to improve the event reconstruction. After alignment and calibration tracks are reconstructed and the topology of the events is determined.

Here, the reconstruction of the primary interaction vertex in the target is an important part of the data analysis. To select a set of tracks originating from the primary vertex a simple and fast preliminary track selection procedure was used. The least-square estimator called the Kalman filter was then employed in a more sophisticated analysis to find the position of the vertex and to force the momentum vectors of tracks to pass through this common point (see fig. 10) A recursive method was used to check the association of tracks with the vertex. Finally the momentum vectors and covariance

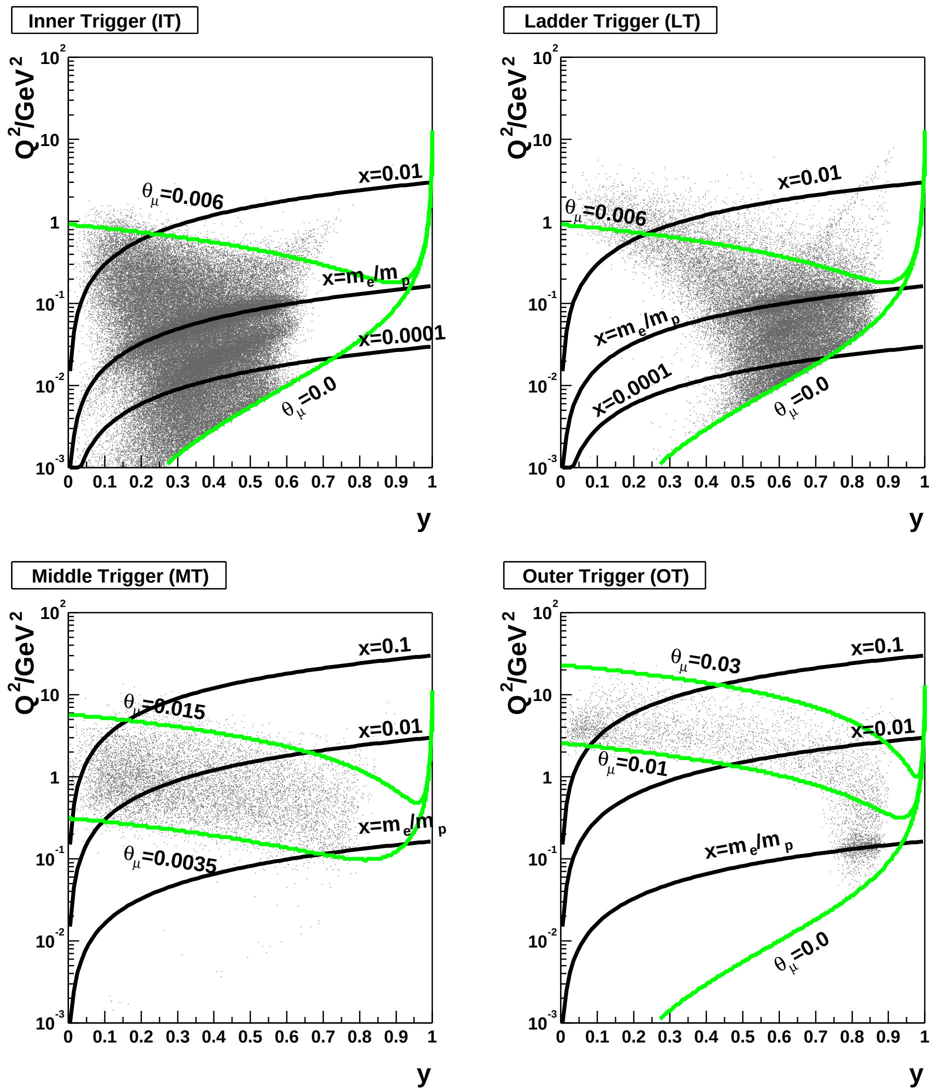

Abb. 8: Event distribution in y and Q^2 for the four trigger subsystems. Here, the inner and the ladder trigger were used with calorimeter condition.

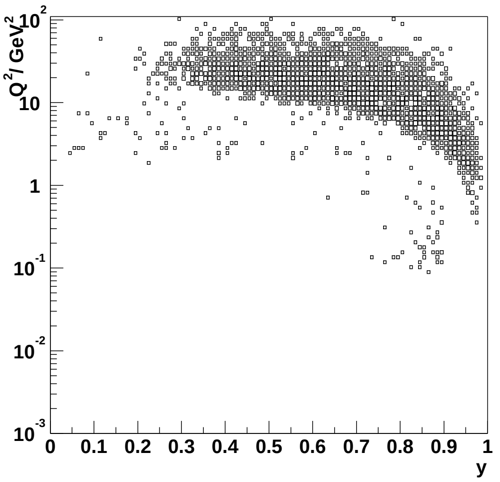

Abb. 9: Event distribution in y and Q^2 for the pure calorimetric trigger. Events with an additional hodoscope trigger were excluded.

matrices of tracks emerging from the interaction point were improved due to the vertex constraint. The vertex coordinate resolution achieved for the Monte Carlo events is of the order of 0.1 mm in the transverse plane and 20.3 mm along the beam direction.

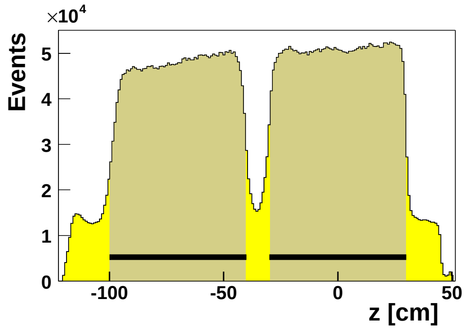

Abb. 10: Distribution of μ interaction vertex reconstructed in COMPASS. Two black bars at bottom indicate two target cells.

The code was written in C++ in the frame of Object Oriented approach to software design. It is integrated into COmpass Reconstruction and AnaLysis program (CORAL), which provides reconstructed tracks for the input of package [6].

Meanwhile the analysis of several physics channels is progressing well, e.g. semi-inclusive asymmetries, ρ and ϕ production, the measurement of $\Delta G/G$, Λ polarisation and transverse asymmetries. The first two subjects will be described in some detail below, while only a short summary is given for the others.

Gluon polarisation

The gluon polarisation, $\Delta G/G$, will be accessed through measurements of the cross section asymmetries in the photon-gluon fusion process ($g\gamma^* \rightarrow q\bar{q}$) tagged either by open charm production of a D^0 ($\bar{D}^0$) or D^{*+} (D^{*-}) meson or by a high tranverse momentum hadron pair in the final state. The former reaction is very clean due to the charmed meson decay in the Kπ channel with the cross section high at low Q^2. The latter is very abundant but flooded by the background of QCD Compton scattering and of the leading order processes.

For open charm production identification of the K with the RICH is essential. For the D^* channel an additional soft π is required. Preliminary signals for D and D^* mesons are shown in fig. 11. The expected accuracy for $\Delta G/G$ after 3 years of data taking (2002-4) is about 0.24.

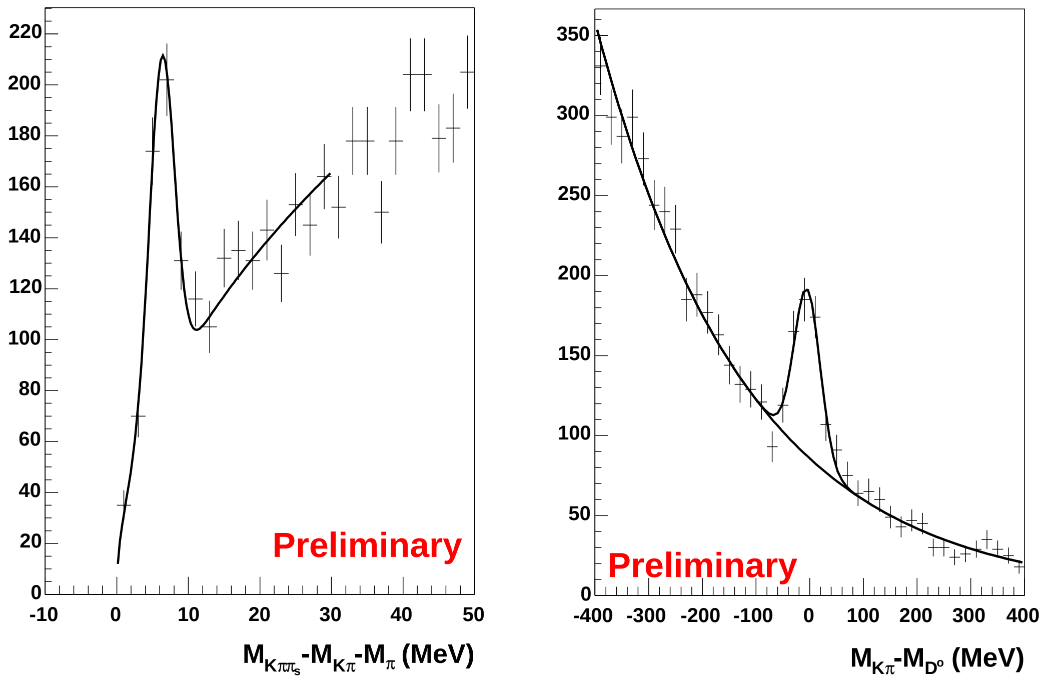

Abb. 11: D^* produced by requiring the invariant mass of the Kπ pair to be in the 6 MeV window aroung the D^0 peak, together with a detected soft pion. Using this D^* cut, the D^0 peak in the invariant mass spectrum of Kπ is very clear.

The second analysis uses events with a primary vertex with a scattered muon and at least two high transvers momentum hadrons ($p_T > 0.7$ GeV/c). To enhance the PGF process additional kinemactical cuts are applied e.g. $x_F > 0.1$ and $(p_{T1}^2 + p_{T2}^2) > 2.5$ (GeV/c)^2. The preliminay result for the measured asymmetry is $A^{\gamma^* d} = -0.065 \pm 0.036(\text{stat}) \pm 0.010(\text{false})$. Here, the second error gives the contribution from false asymmetries only, the other sources of systematic uncertainties are still being investigated.

Longitudinal polarisation of the Λ hyperon

Longitudinal polarisaiton of the Λ in the current fragmentation region provides a possibility to measure the spin transfer in the fragmentation as well as to test the strange sea symmetry in the nucleon. The Λs are clearly identified in the data (see fig. 12) by their secondary vertex outside the target and the πp decay. Their polarisation was measured via the angular distribution $\mathrm{d}N/\mathrm{d}\cos\theta_i$ of the positive decay products. Figure 12 shows the results for the ratio of measured to simulated angular distributions from 1/6 of the 2002 statistics. Here an unpolarised Monte Carlo was used. As expected there is no deviation from flatness for the spinless K^0 and $\cos\theta_z$ for the Λ and $\bar{\Lambda}$.. The data demonstrate the good COMPASS potential for the Λ polarisation measurements.

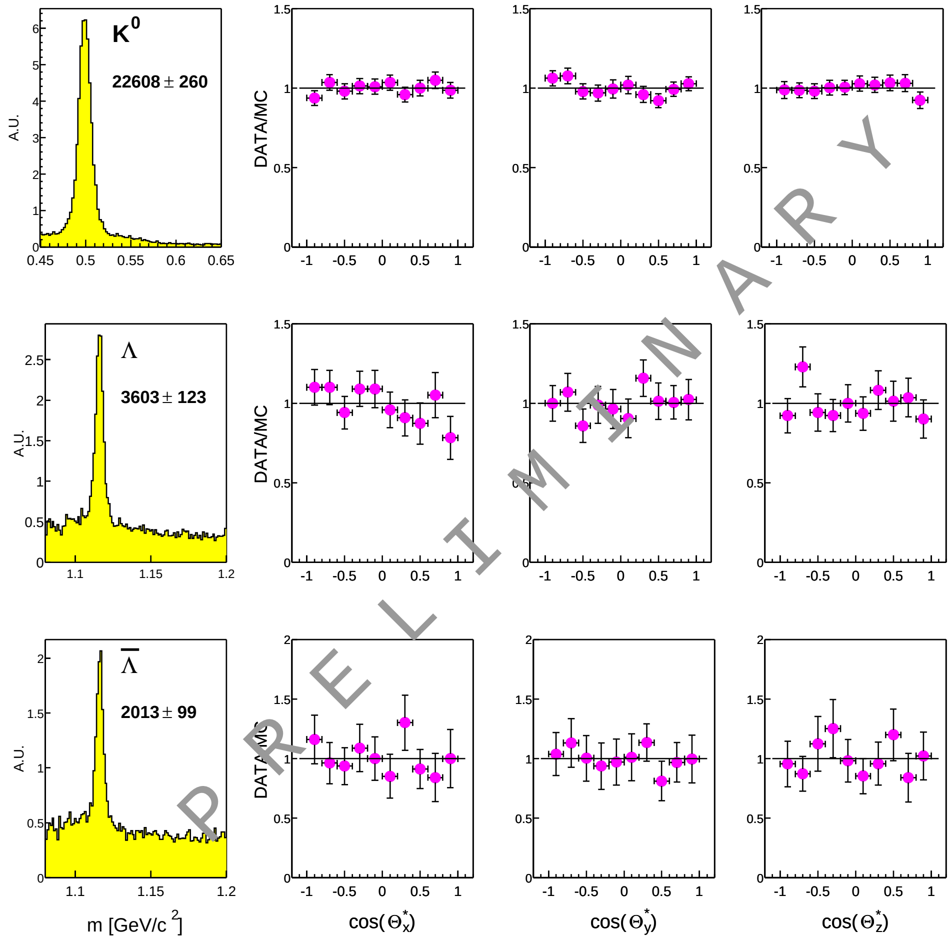

Abb. 12: Angular distributions of K^0, Λ and $\bar{\Lambda}$ normalised to the (unpolarised) Monte Carlo simulations. Errors are statistical. The first column shows the K^0, Λ and $\bar{\Lambda}$ invariant mass distributions.

Collins asymmetry and transversity

Semi-inclusive deep inelastic scattering off a transversely polarised target permits to measure the transverse spin dependent parton distributions $\Delta_{\mathrm{T}}q(x)$ via the azimuthal dependence of the leading hadrons (Collins angle ϕ_{C}). In 2003 about 10^7 events were collected with the transversly polarized target in the $Q^2 > 1$ (GeV/c)^2 region. Figure 13 shows the results for the x and z dependence of the collins asymmetry for positive and negative hadrons. As can be seen the asymmetries are small and compatible with 0 in the low x region where sea quarks dominate.

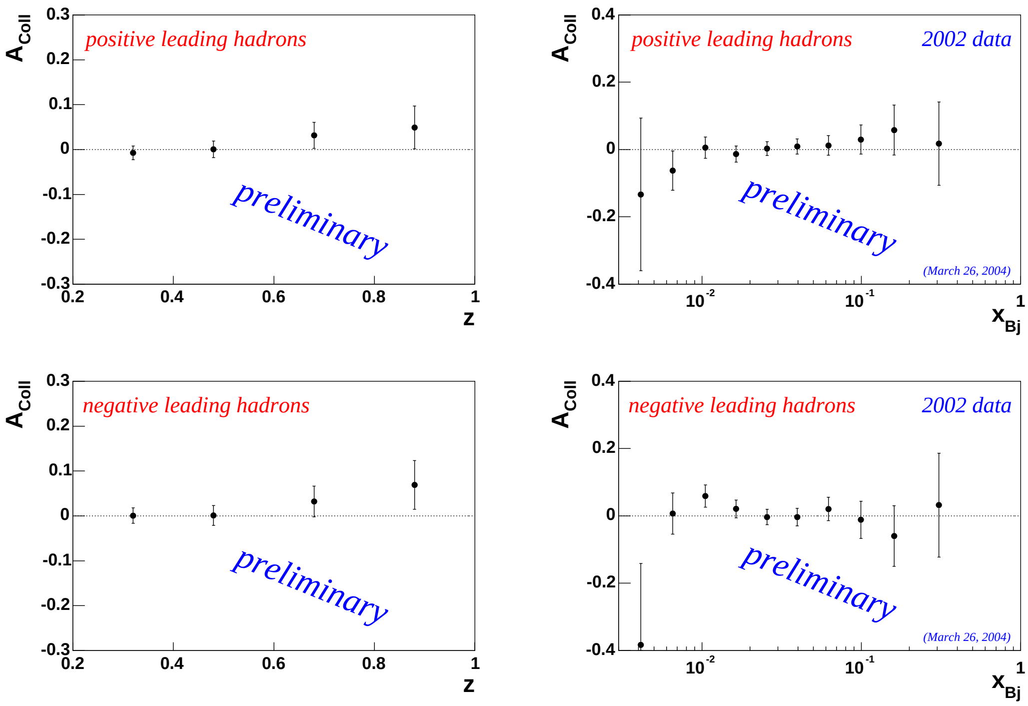

Abb. 13: top: Collins asymmetry vs. z and x for positive hadrons, bottom: Collins asymmetry vs. z and x for negative hadrons. Error bars are statistical error only.

Semi-inclusive double-spin asymmetries in COMPASS

In parallel to the ΔG measurement the measurement of polarized parton distributions Δq can be performed in COMPASS [6]. Δq can be extracted via study of semi-inclusive DIS asymmetries when in addition to the scattered muon μ a hadron h is detected:

$$\vec{\mu} \ + \ \vec{N} \rightarrow \mu' \ + \ X \ + \ h$$

Tagging events with a certain hadron allows to determine the flavor of the struck quark. For instance observation of strange particle manifest by itself that s-quark took part in the process. If written in the leading order of QCD the double-spin asymmetry for hadrons is a linear combination of quark and anti-quark helicity distributions:

$$A_1^h = \frac{\sum_q e_q^2(\mathbf{\Delta q(x)} \int D_q^h(z)dz + \mathbf{\Delta \bar{q}(x)} \int D_{\bar{q}}^h(z)dz)}{\sum_q e_q^2(q(x) \int D_q^h(z)dz + \bar{q}(x) \int D_{\bar{q}}^h(z)dz)}$$

where $q(x)$ and $\int_{0.2}^{1} D_q^h(z)dz$ are non-polarized quark distributions and hadron fragmentation functions respectively.

We will measure six asymmetries. They are $\vec{A}_1$=$\{A_1,\ A_1^{h+},\ A_1^{h-},\ A_1^{K+},\ A_1^{K-},\ A_1^{K_S^0}\}$. The inclusive spin asymmetry A_1 was measured already by many experiments and can serve as a crosscheck for the obtained results. In addition, with the full statistics COMPASS can increase precision in low x region. A_1^{h+}, A_1^{h-} are positively and negatively charged hadron asymmetries. Note that 90% of hadrons are pions. Using RICH particle identification we can tag events with produced charged kaons. Kaon asymmetries A_1^{K+}, A_1^{K-}, $A_1^{K_S^0}$ play essential role in Δs determination since kaons carry strangeness inside.

However having ^{6}LiD target only limited flavor separation is possible. The isospin symmetry of deuteron allows us to select three parton combined densities $\vec{\Delta q}$=$\{\Delta u+\Delta d,\ \Delta\bar{u}+\Delta\bar{d},\ \Delta s\}$, where it is assumed that $\Delta s = \Delta\bar{s}$. With aid of minimization routing $\vec{\Delta q}$ can be extracted having as an input $\vec{A}_1(x)$, $q(x)$ and $D_q^h(z)$. For non-polarized distributions the world global data will be used [8]. Hadron fragmentation functions will be taken either from EMC measurements or calculated with MC generators. If combined with results on proton target full flavor separation is possible: $\vec{\Delta q}$=$\{\Delta u,\ \Delta\bar{u},\ \Delta d,\ \Delta\bar{d},\ \Delta s,\ \Delta\bar{s}\}$.

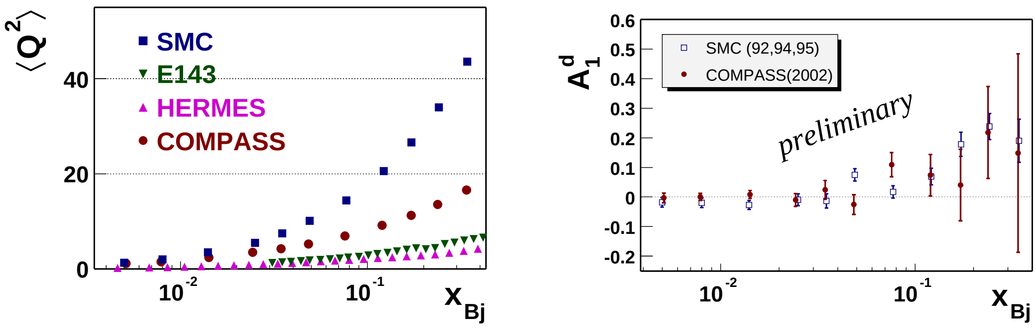

Abb. 14: *Left*: comparison of COMPASS $\langle Q^2\rangle$ with other experiments. *Right*: inclusive A_1 asymmetry measured in COMPASS superposed by SMC points.

Inclusive asymmetries were obtained from the 2002 data with longitudinally polarised target. In fig. 14 $\langle Q^2\rangle$ is presented in comparison with other experiments. The COMPASS $\langle Q^2\rangle$ values are a factor of two lower than the SMC ones, but a factor of 2-3 higher than the ones of E143[9] and HERMES.

Figures 14 shows the results for $A_1^{\rm d}$ compared to the previous SMC results [7]. The kinematicsl cuts of $0.1 < y < 0.9$ and $Q^2 > 1$ GeV$^2/c^2$ have been applied leading to x interval of $0.003 < x < 0.4$. The SMC measurement is still more precise in the region of $x > 0.1$, for low x COMPASS has the same statistical errors as SMC with only one year of data taking.

Exclusive ρ^0 and ϕ production in COMPASS

Unpolarised leptoproduction of various vector mesons has been extensively investigated in a wide range of energy, both at fixed target experiments and at HERA [13]. The data cover large range of from quasi-photoproduction to the deep inelastic domain (up to $Q^2 \approx 30\,\mathrm{GeV}^2$). Analysing data from run 2002 COMPASS obtained first preliminary results on exclusive ρ^0 and ϕ production. We investigate the elastic vector meson (VM) production passing via coherent $\mu + A \to \mu + A + VM$ scattering, where A is the nucleus, which remains intact in the final state and incoherent $\mu + N \to \mu + N + VM$ scattering, where N is the target nucleon, which can be either free or bound in the nucleus. We study reactions with ρ^0 or ϕ mesons in the final state decaying via the hadronic mode ($\pi^+\pi^-$ and K^+K^- respectively). The high beam luminosity results in the large statistics which even with one year of data taking will allow to reduce significantly the errors on both unpolarized and polarized observables. In addition, an extended range at low Q^2, compared to other fixed target experiments, will allow to explore the region close to the photoproduction.

meson	mass cut	statistics (1/6 of 2002)
ρ^0	$0.5 < m_{\pi\pi} < 1$ GeV	$1.3 \cdot 10^6$
ϕ	$\lvert m_{KK} - m_\phi \rvert < 9$ MeV	$42 \cdot 10^3$

Tab. 1: The preselected sample statistics.

To increase the purity of the sample the following kinematical selections are applied. To decrease the contribution of non-exclusive background in the sample we apply a cut on the transverse momentum transfer: $-t' < 0.5$ (GeV/c)^2. In order to suppress not-exclusive events which exhibit the topology of exclusive events a cut on the missing energy ΔE has been applied, where $\Delta E = (M_X^2 - M_p^2)/2M_p$ and M_X is the missing mass of undetected final state particles. ΔE is a measure of exclusivity. They are beam track, scattered muon and two hadrons of opposite charge. We define the sample of exclusive events by requiring $-2 < \Delta E < 2.5$ GeV. The total numbers of events for certain mass intervals in the preselected sample are presented in table 1.

The kinematic range is $10^{-3} < Q^2 < 10$ GeV$^2/c^2$ and $7.5 < W < 16$ GeV. The sample is dominated by quasi-real photoproduction and the energy W is outside of the photon-nucleon resonance region.

As usual for the region near to photoproduction we observe a skewing of the ρ^0 invariant mass distribution compared to the relativistic Breit-Wigner shape. The enhancement of events at low masses and the depletion at large masses can be described by the Söding model [10] as an interference between resonant ρ^0 production and "Drell-type" background processes. This background is coming from the fluctuations of the virtual photon into two pions which scatter diffractively on the proton. The mass spectrum has been fitted with an expression corresponding to the coherent sum of resonant and non-resonant $\pi^+\pi^-$ production [11]. Fig. 15 shows the results of the fit for different intervals of t' (top row) and Q^2 (bottom row).

ρ^0 and ϕ are vector mesons which decay into two spinless hadrons. Their spin state will be reflected in the orbital angular momentum of decay mesons. The detailed formalism can be found in [12]. Usually the VM decay angular distribution $W(\cos\theta, \phi, \Phi)$ is studied in the s-channel helicity frame, which is the most convenient for describing the VM decay after photo- and electroproduction [13]. In this analysis we consider only one-dimensional projections of the angular distributions. The Q^2 range is split into four

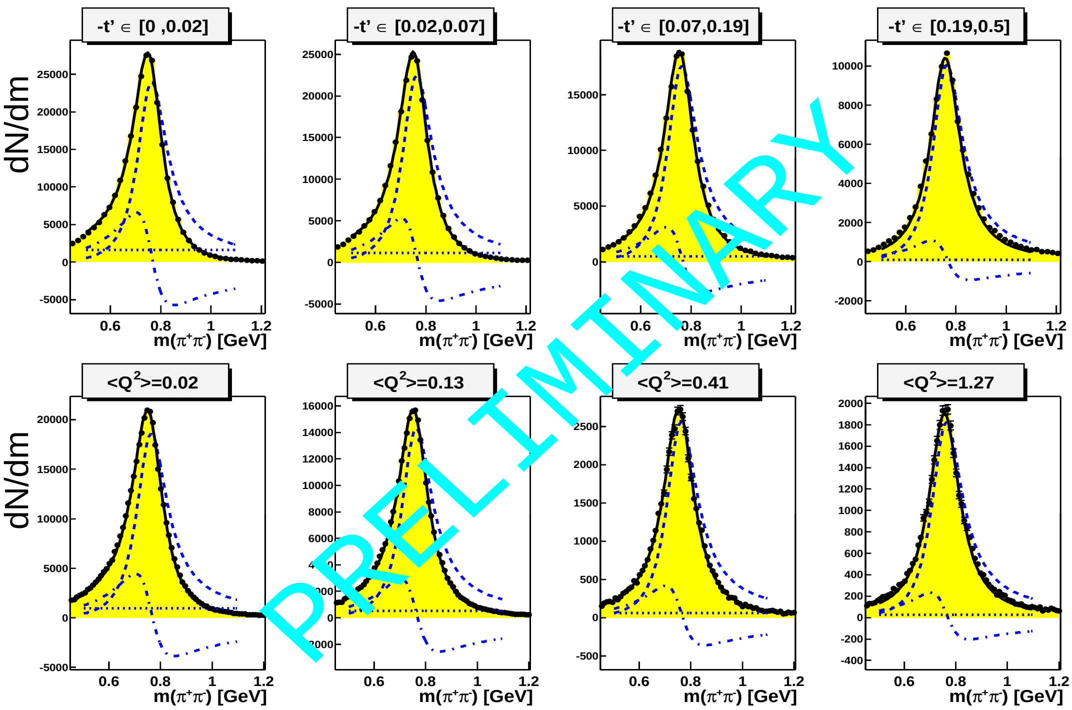

Abb. 15: The fit of ρ^0 invariant mass distribution according to Söding parameterization. *Dashed line* corresponds to relativistic p-wave Breit-Wigner resonant contribution, *dotted line* – non-resonant part, *dashed-dotted* – interference term. No acceptance corrections were applied.

slices[1]. Fig.16 shows the $\cos\theta$ and ψ distributions for the ρ^0 case ($\psi = \phi - \Phi$). One can see that at small Q^2 the distribution of $\cos\theta$ has $\sin^2\theta$ - like dependence which indicates that production of transversely polarized (helicity ± 1) VM dominates. At large Q^2, when the contribution from interaction of longitudinally polarized photons dominates, the distribution changes the curvature and has $\cos^2\theta$ - like shape. The modulation in ψ relates to the contribution from the production of transverse photons. The fact that it peaks at 0 and π indicates that the decay mesons are mainly emitted in the muon scattering plane. The assumption of SCHC and natural parity exchange in t channel applies constrain on ψ modulation amplitude resulting to the vanishing of the latter in the region of longitudinal VM production (high Q^2).

The large statistics expected in COMPASS will allow to reduce significantly the errors on unpolarized and polarized observables for exclusive ρ^0 and ϕ channels. In addition, the extended range of low Q^2, compared to other fixed target experiments, will allow to explore the region close to the photoproduction.

[1] G. Baum et al., COMPASS-Proposal, CERN/SPSLC/96-14; SPSLC/P297.

[2] for more details see:
http://wwwcompass.cern.ch/compass/detector/trigger/muon-trigger

[3] A. Bravar et al., Jahresbericht 1998/1999.

[1]For the current analysis we apply the cut $Q^2 > 0.05$ (GeV/c)^2 to remove events with small scattering angles where angular smearing effect become essential.

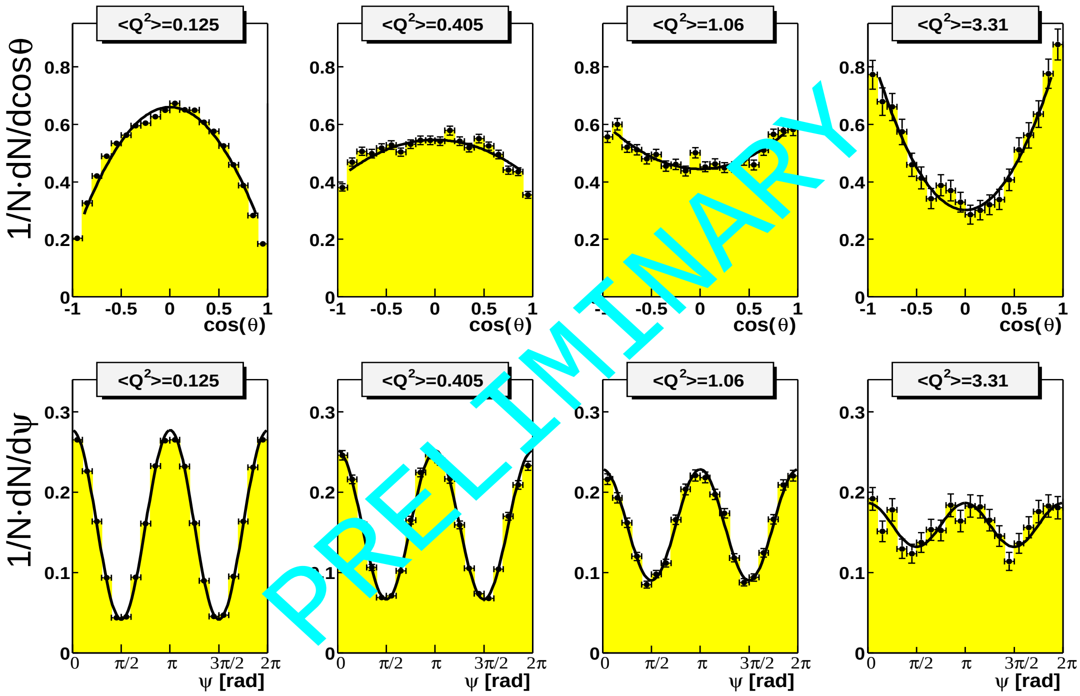

Abb. 16: ρ^0 angular distributions for different Q^2 intervals. No acceptance and angular smearing corrections were applied. Only statistical errors are shown.

[4] R. Hermann, Diploma thesis, Mainz 2003.

[5] M. Leberig, PhD thesis, Mainz 2002.

[6] A. Korzenev, PhD thesis, in preparation.

[7] B. Adeva et al., Phys. Rev. D 58 (1998) 112001.

[8] D. Stump et al., hep-ph/0303013

[9] K. Abe et al., hep-ph/9802357

[10] P. Söding, Phys. Lett. 19 (1966) 702.

[11] ZEUS Collab., M. Derrick et al., Z. Phys. C69 (1995) 39.

[12] K. Schilling and G. Wolf, Nucl.Phys. B61 (1973) 381.

[13] T.H. Bauer et al., Rev. Mod. Phys. 50 (1978) 261.